Marian Klasztorny[1]*, Daniel Bronisław Nycz[2], Kamil Paweł Zając[1]

[1] Military University of Technology, Faculty of Mechanical Engineering, Department of Mechanics and Applied Computer Science
ul. gen. W. Urbanowicza 2, 00-908 Warsaw, Poland
[2] Jan Grodek State Vocational Academy, Institute of Technology, ul. S. Reymonta 6, 38-500 Sanok, Poland
*Corresponding author. E-mail: marian.klasztorny@wat.edu.pl

ENHANCED MODELLING AND NUMERICAL TESTING OF GFRP COMPOSITE BOX BEAM WITH ADHESIVE JOINTS

The subject of the experiment and numerical research is a simply-supported thin-walled box beam with a span of 2.00 m, created by gluing two composite GFRP shells. The beam was subjected to a three-point bending test controlled by displacement in the range from 0 to 300 mm. An experimental bending test, numerical modelling and simulations of this test as well as validation of the modelling and simulation were carried out. In comparison with the authors' previous publication, adjustments and enhancements include: correction of the GFRP material constants and friction coefficients; testing the key numerical parameters of the geometrically and physically non-linear task, i.e. an iteration step in the implicit algorithm, a convergence tolerance coefficient, FE mesh density; testing the use of the *Glue* contact option in the MSC.Marc FE code for modelling adhesive joints; quasi-optimization of the ply sequence with the maximum load bearing capacity as the objective function. The parameters and options of numerical modelling and simulation of glued composite shells in the MSC.Marc system were determined, useful for detailed design calculations of composite FRP structures.

Keywords: GFRP composite shells, adhesive joints, three-point bending test, numerical modelling and simulation, experimental validation, numerical testing

ULEPSZONE MODELOWANIE I BADANIA NUMERYCZNE BELKI SKRZYNKOWEJ Z KOMPOZYTU GFRP ZE SPOINAMI KLEJOWYMI

Przedmiotem badań numerycznych jest cienkościenna belka skrzynkowa swobodnie podparta, o rozpiętości 2.00 m, utworzona przez sklejenie dwóch powłok kompozytowych GFRP ze sobą na całej długości belki. Belkę poddano próbie trójpunktowego zginania sterowanego przemieszczeniem w zakresie od 0 do 300 mm. Przeprowadzono eksperymentalną próbę zginania, modelowanie numeryczne i symulacje tej próby oraz walidację modelowania i symulacji. W porównaniu z poprzednią pracą autorów (Composites Theory and Practice, 2015) korekty i ulepszenia obejmują: korektę stałych materiałowych kompozytu GFRP i współczynników tarcia, testowanie parametrów numerycznych zadania nieliniowego geometrycznie i fizycznie, tj. krok iteracyjny w algorytmie implicite, współczynnik tolerancji zbieżności, gęstość siatki elementów skończonych, testowanie opcji Glue contact w systemie MSC.Marc do modelowania spoin klejowych, quasi-optymalizacja sekwencji warstw z funkcją celu w postaci maksimum nośności belki przy zginaniu. Wyznaczono parametry i opcje modelowania numerycznego i symulacji kompozytowych powłok sklejanych z użyciem systemu MSC.Marc, przydatne do szczegółowych obliczeń projektowych konstrukcji z kompozytów FRP.

Słowa kluczowe: powłoki kompozytowe GFRP, spoiny klejowe, test trójpunktowego zginania, modelowanie numeryczne i symulacja, walidacja eksperymentalna, badania numeryczne

INTRODUCTION

Footbridges made of innovative FRP composite materials offer a number of desirable features, including high strength-to-mass and stiffness-to-mass ratios, good fatigue performance and high resistance to moisture, corrosion, weather factors and UV radiation, as well as a relatively long service life with minimal maintenance costs.

In order to properly predict the ultimate strength of the laminate in a complex stress state, an adequate failure criterion must be adopted. To date, a number of failure criteria have been formulated, among others, the *maximum stress, maximum strain, Tsai-Wu, Hashin, Hashin Fabric, Tsai Hill, Hoffman, Chang-Chang, Hill* and the *Malmeister* criterion. The *Hashin Fabric* criterion with its progressive damage procedure gives a reasonably good damage and failure prediction of FRP laminates [1].

The numerical modelling and simulation of selected FRP composite beams has been developed by a number of researchers, e.g. [2-6]. Kubiak and Kaczmarek [2]

presented the numerical and experimental investigations of GFRE/CFRE thin-walled channel columns loaded till failure. Kubiak et al. [3] presented the experimental investigations of GFRE thin-walled channel columns subjected to static compression, using the acoustic emission method to investigate the behaviour prior to collapse. Experimental validation of the FE model of the columns is conducted in order to analyse the post-buckling behaviour and to determine the failure load with the well-known failure criteria. Gliszczynski and Kubiak [4] presented an estimation of the load capacity of composite channel columns subjected to uniform compression. The columns were made of GFRP laminate with selected symmetric ply sequences. The numerical modelling and simulation were performed using ANSYS® FE code.

Klasztorny et al. [5, 6] developed the numerical modelling and simulation of GFRP laminates based on beam and plate specimens made of balanced plain weave fabrics and mats, fabricated using hand lay-up technology.

The numerical modelling and simulation methodology for U-type sandwich footbridges was developed by Chroscielewski et al. as part of the research project entitled FOBRIDGE, financed in the years 2013-2015 by the National Centre for Research and Development, Poland [7]. The authors used the ANSYS system. The numerical modelling and simulation methodology for box footbridges of a selected type was developed by Klasztorny et al. as part of the same project [8]. In both structural solutions laminate shells were fabricated using stitched balanced orthogonal fabrics of an 800 g/m² mass density and fire retardant vinyl ester resin.

Numerical modelling and simulation of the box-type superstructure of the pedestrian-and-cyclist bridge designed in [8] was validated experimentally with the three-point bending test of an adhesively bonded box beam [9]. The validation beam reflected the central box of the footbridge superstructure, on a 1:2 scale and after turning the segment by 180°.

Compared to [9], the present work has improved and extended numerical tests of the box beam in the form of two shells glued together along the whole beam length, subjected to a three-point bending test, using MSC.Marc FE code. The adjustments and enhancements include:
- correction of the dimensions of the reference surface,
- correction of the GFRP material constants and friction coefficients,
- testing the key numerical parameters of the geometrically and physically non-linear task, i.e. a displacement increment in the implicit algorithm, an iteration accuracy coefficient, FE mesh density,
- testing the use of the *Glue* contact option for modelling the adhesive layer,
- the influence of selected ply sequences on the load capacity of the box beam.

ADHESIVELY BONDED JOINTS IN FRP COMPOSITE STRUCTURES

The state of scientific and technological knowledge on the joints of adhesively bonded shells or sandwich shells fabricated using FRP composites is presented by Banca and Silva [10]. The glued joints considered in the literature adhesively bond two shells on a small surface in the form of a single-lap joint, double-lap joint or other. They are connections perpendicular to the direction of joint loading, mainly work under shear and are exposed to stress concentrations at the joint edges.

In this work, the connection of two FRP composite shells in the joint loading direction, i.e. over the entire length of the beam, is considered. Such a connection mainly works under tension or compression and is not exposed to stress concentrations.

The advantages of adhesively bonded FRP composite shells compared to conventional mechanical joints are as follows:
- avoiding screw holes,
- avoiding interruption of fibre continuity,
- avoiding the concentration of stresses and shear in the area of screw holes,
- uniform transfer of stresses through the adhesive layer in the case of a suitably shaped system of shells glued together,
- ease of making adhesively bonded joints,
- increasing the load capacity of the structure,
- ensuring long-term durability of the structure,
- reducing the weight of the structure,
- reducing the costs of manufacturing the structure.

In order to obtain an adhesively bonded joint with high strength and long durability, FRP composite shells with a thermosetting matrix require mechanical processing, which includes [11]:
- cleaning and degreasing of the surfaces to be adhesively bonded,
- abrasive treatment of the surfaces to be adhesively bonded.

Structural adhesives form chemical bonds with such treated FRP composite shells if the adhesive is chemically compatible with the resin matrix.

The adhesive for joining vinyl ester-glass shells should have the following properties:
- chemical compatibility of the glue with the vinyl ester matrix of the glued shells,
- curing temperature of the adhesively bonded joint: 50°C,
- relatively high cohesive and adhesive tensile strengths,
- relatively high cohesive and adhesive shear strengths,
- a relatively long glue gelling start time,
- operating temperature range of joints: [−30°C, +45°C],
- high resistance to humidity and vibrations.

The construction adhesive NORPOL FI-184® (producer: Reichhold, Norway) was selected from the market offer, which meets the above requirements. It is an isotropic material based on vinyl ester, intended for gluing polyester/vinyl ester shells, it has an incorpo-

rated accelerator and changes from light grey to yellow-ish brown after addition of the initiator. The adhesive is suitable for machine application at temperatures from 18 to 25°C.

DESCRIPTION OF GFRP COMPOSITE BEAM, CONSTRUCTION MATERIALS AND TEST STAND

The object of experimental and numerical research is a box beam made of two composite shells, a vinyl ester-glass laminate, shown in Figure 1. The laminate matrix is the vinyl ester resin BÜFA Firestop S 440 (producer BÜFA Gelcoat Plus Co., Germany). Biaxial balanced stitched E-glass fabrics BAT800 [0/90] and GBX800 [45/–45], of an 800 g/m^2 mass density (producer DIPEX, Slovakia) were used. These FRP components were applied in the project FOBRIDGE [7, 8]. The reference symmetric ply sequence is as follows: [BAT/GBX/2BAT/GBX/BAT], wherein the fabrics are unrolled along the beam length.

The lamina designated as BG/F corresponds to one BAT or GBX fabric. The material model of the laminae is orthotropic linear elastic-brittle. The material constants of lamina BG/F were determined in [12] for the new material under normal conditions (RT, 50% humidity) and are listed in Table 1. The following symbols were introduced:

1,2,3 - directions of orthotropy of the composite reinforced with BAT800 or GBX800 fabric, i.e. warp direction, weft direction and thickness direction, respectively,

E_1, E_2, E_3 - Young's modules in the directions of orthotropy,

G_{12}, G_{13}, G_{23} - shear modules in the orthotropic planes,

$\nu_{12}, \nu_{23}, \nu_{31}$ - Poisson's coefficients in the orthotropic planes, with $\dfrac{\nu_{ij}}{E_i} = \dfrac{\nu_{ji}}{E_j}$, $i, j = 1,2,3$,

R_{1t}, R_{2t}, R_{3t} - tensile strengths in the directions of orthotropy,

R_{1c}, R_{2c}, R_{3c} - compressive strengths in the directions of orthotropy,

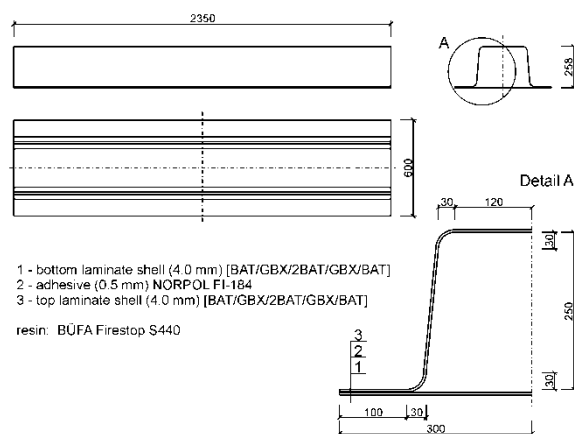R_{12}, R_{13}, R_{23} - shear strength in the orthotropic planes.

Material constant, unit	Symbol	Value
Young's modules [MPa]	$E_1 = E_2$	23 400
Young's modulus [MPa]	E_3	7 800
Poisson's ratio in plane 12	ν_{12}	0.153
Poisson's ratio in plane 23	ν_{23}	0.593
Poisson's ratio in plane 13	ν_{31}	0.197
shear modulus [MPa]	G_{12}	3 500
shear modules [MPa]	$G_{13} = G_{23}$	1 400
tensile strengths [MPa]	$R_{1t} = R_{2t}$	449
compressive strengths [MPa]	$R_{1c} = R_{2c}$	336
shear strength in plane 12 [MPa]	R_{12}	45
shear strengths in planes 13, 23 [MPa]	$R_{13} = R_{23}$	35

The adhesive material model is isotropic linear elastic-brittle. The following values of material constants of the NORPOL FI-184 adhesive, cured at RT for 24 h and at 50°C for 24 h, were adopted on the basis of the product data sheet submitted by the producer (Reichhold, Norway):
- tensile and compressive strength $R_t = R_c = 35$ MPa
- shear strength $R_s = 14.4$ MPa
- ultimate elongation at stretching $e_u = 3.5\%$
- Young's modulus $E = 3.1$ GPa
- Poisson's ratio $\nu = 0.36$
- heat distortion temperature HDT = 65°C

A diagram of the test stand for the three-point bending test of the box beam is presented in [9]. The simply-supported beam is loaded with a displacement-controlled crosshead from 0 to 300 mm, at the velocity of 1 mm/s. The values of vertical displacement and pressure force on the beam were automatically recorded with the frequency of 10 Hz. The test was carried out on a SATEC 1200® universal testing machine, in the Laboratory of Strength of Materials, Department of Mechanics and Applied Computer Science, Faculty of Mechanical Engineering, Military University of Technology, Warsaw, Poland.

NUMERICAL MODELLING OF BOX BEAM SUBJECTED TO BENDING TEST

The geometry of the box beam, shown in Figure 1, was reproduced by the reference surface as in Figure 2, with the following indications: L - laminate, G - glued joint. The arrows show the position of G, L relative to the reference surface.

The numerical model of the box segment was built in two variants: BB1 - a model in which the adhesive is a layer of a 13-layer laminate in the flange zone; BB2 - a model in which the adhesive was modelled by a *Glue* contact between 6-layer laminates. The reference surface was meshed with finite elements of QUAD4 topol-

Fig. 1. Adhesively bonded GFRP composite box beam
Rys. 1. Belka skrzynkowa z kompozytu GFRP ze spoinami klejowymi

1 - bottom laminate shell (4.0 mm) [BAT/GBX/2BAT/GBX/BAT]
2 - adhesive (0.5 mm) NORPOL FI-184
3 - top laminate shell (4.0 mm) [BAT/GBX/2BAT/GBX/BAT]

resin: BÜFA Firestop S 440

ogy, with an average size of 15 mm (Fig. 3) [1]. This is the basic mesh (11 088 finite elements, 11 176 nodes). Meshing of the beam model was performed in the Altair HyperMesh® 2017.2 programme.
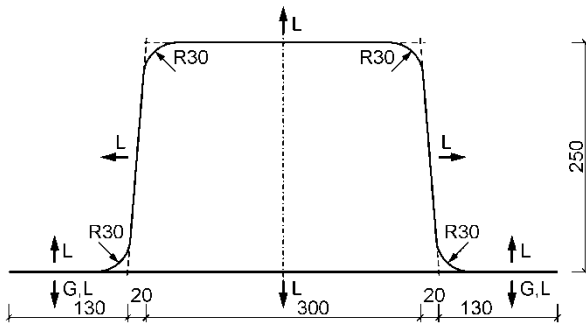

Fig. 2. Cross-section of box beam reference surface

Rys. 2. Przekrój poprzeczny powierzchni referencyjnej belki skrzyn-
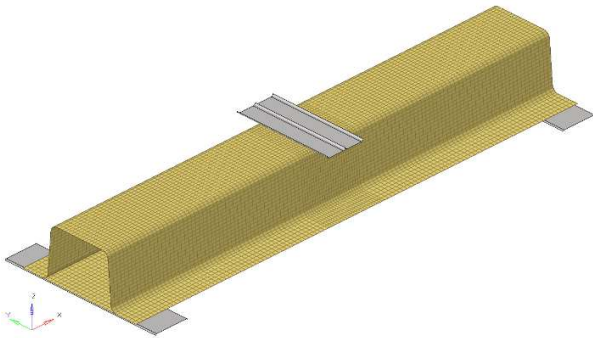kowej

Fig. 3. Numerical model of box beam subjected to three-point bending
test (basic mesh)

Rys. 3. Model numeryczny belki skrzynkowej poddanej testowi trój-
punktowego zginania (siatka podstawowa)

The finite elements were assigned the formulation *Bilinear Thick-shell Element* (No. 75). They are bilinear, two-dimensional, 4-node *Thick Shell* finite elements with three translational and three rotational degrees of freedom in each node [1]. Two material models were defined:
- orthotropic model of vinyl ester-glass lamina BG/F (Table 1),
- adhesive isotropic model (only for the BB1 model).

For the orthotropic lamina BG/F, the *Hashin-Fabric* failure criterion was defined [1]. This criterion is a variant of the *Hashin* failure criterion for use in a lamina reinforced with an orthogonal fabric. At each integration point, the MSC.Marc system calculates six failure indexes defined in Ref. [1] and discussed in Ref. [9]. The effort indices at a given integration point are equal [1]

$$R_i = \sqrt{F_i}, \quad i = 1, 2, 3, 4, 5, 6 \qquad (1)$$

For the *Hashin Fabric* criterion, the *Selective Gradual Degradation* progressive failure model, implemented for composites and other elastic materials in the MSC.Marc system, was adopted. This model reduces

the elastic modules accordingly at the initiation of failure. For particular finite elements, the orientation of the material properties of the laminae was declared in the *Material Properties/Orientations* table [1].

In the BB1 model, for the adhesive layer, the *Hashin Fabric* failure criterion was also adopted, treating the isotropic material of the adhesive as a special case of the orthotropic material. This criterion corresponds to the adhesive failure model adopted for the *Glue* contact [1].

A total effort contour map (TECM) covers all the laminae and is defined by the formula

$$R = \max_{i,j} \left[R_i, \quad i = 1, 2, \ldots, 6, \; j = 1, 2, \ldots, n \right] \quad (2)$$

where n denotes the total number of laminae at a given laminate middle surface point.

Due to the many times higher stiffness of the supports and pressing block compared to the stiffness of the laminated thin-walled beam, the support and crosshead are modelled using a surface with perfectly rigid body properties. A contact table was used to define the *Touching* contact, in which the potential contact between individual parts of the model was declared. The Coulomb friction model with coefficients of friction $\mu = 0.09$ for a steel-laminate pair and $\mu = 0.25$ for a laminate-laminate pair was used in the analyses. The values of the friction coefficients were determined from the authors' own experimental tests.

For the BB2 model, *Glue* contact was introduced for the box beam flange, with failure parameters R_t, R_s given in given in the paragraph under Table 1. Adhesive failure of the glue occurs if [1]

$$\left(\frac{\sigma}{R_t}\right)^m + \left(\frac{\sigma_s}{R_s}\right)^n > 1 \qquad (3)$$

where σ is normal stress, and σ_s - shear stress relative to the contact surface, with $m = n = 2$ which corresponds to the *Hashin-Fabric* criterion.

The simulation takes into account gravity (*Gravity Load*), via declaring an acceleration of -9810 mm/s² relative to the Z axis of the global coordinate system, for all elements of the model. The box beam deflection was determined under its own weight. The box beam-supports-pressing block system is bisymmetric. The bisymmetry was taken into account by withdrawing the appropriate degrees of freedom in the vertical planes of symmetry, i.e. displacements in the direction of the X axis in the transverse plane and displacements in the Y direction in the longitudinal plane.

The task is non-linearly elastic with failure, due to the supports and the pressing block in the form of unilateral constraints with friction, as well as carrying out the bending test with exceeding the load capacity point and progressive failure of the laminate shells. The full Newton-Raphson method and force convergence criterion were used to simulate the three-point bending test of the beam. Small deformations and high rotations were taken into account.

DETERMINING SIMULATION PARAMETERS

The simulation parameters covered by the numerical analysis are as follows: increment in the crosshead vertical displacement and convergence tolerance coefficient. The values of these parameters, leading to the best compatibility of the simulation with the experiment (validation), were determined for the box beam BB1 model.

We introduce the following designations: F - crosshead pressure force on the beam, s - vertical displacement of the crosshead, s_{max} = 300 mm - maximum vertical displacement of the crosshead, Δs - increment in crosshead displacement, $d = \Delta s/s_{max}$ - relative increment in crosshead displacement, c - convergence tolerance (*conv* parameter in the MSC.Marc system [1]). Figures 4-6 show $F(s)$ graphs corresponding to increments d = 0.010, 0.005, 0.001 and tolerances c = 0.10, 0.05, 0.01.

The following conclusions can be drawn from Figures 4-6:

1. The experimental beam response to the crosshead pressure force controlled by displacement is quasi-linear elastic up to the load capacity point of the beam. After exceeding this point, the progressive failure of the beam starts with a local load increase and again a load decrease. At very large displacements of 250÷300 mm there is great strengthening of the beam caused by shear blocking of the hat-shaped part (top shell). There was no damage to the bottom shell or adhesive joint. After removing the load (withdrawing the crosshead upwards at a constant speed of 1 mm/s), the beam regained its original shape.

2. All the $F(s)$ simulation graphs for selected pairs of d, c parameters can be considered fairly qualitatively and quantitatively compatible with the experimental test, except for the extreme pair (the smallest value of d = 0.001, the highest value of c = 0.10). For all other d, c pairs there is a deviation up or down of the load capacity point in comparison with the experimental graph. The results indicate the advisability of additional simulations for d = 0.040 in order to improve the compliance of the load capacity point with the experimental result.

3. The gradient of the $F(s)$ simulation graphs and the experimental graph is consistent, which indicates that the Young's modules of the lamina are determined with high accuracy and there is negligible influence of material-geometric imperfections. The shift of the simulation response in relation to the experimental one by a few millimetres in the quasi-linearly elastic zone indicates that the experimental values of shear modules G_{13}, G_{23} were underestimated. Alternative methods should be sought to identify these modules than the short beam method used in [12].

4. The simulation of the beam response in the progressive failure zone is approximate. The adopted *Hashin Fabric* failure hypothesis combined with the

of gradual degradation option does not give the possibility to accurately model the experiment. Nevertheless, the main trend of progressive beam failure was modelled correctly. It should be noted that engineering structures (among others, footbridges) work in the range of ~ up to 30% of the load capacity. It is therefore important to only determine the load capacity point with good accuracy.
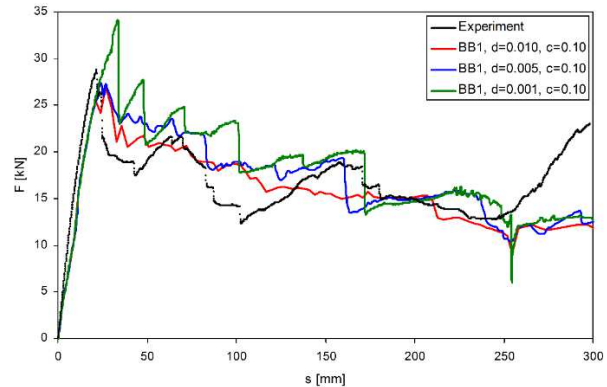

Fig. 4. $F(s)$ graphs corresponding to increments d = 0.010, 0.005, 0.001 and tolerance c = 0.10

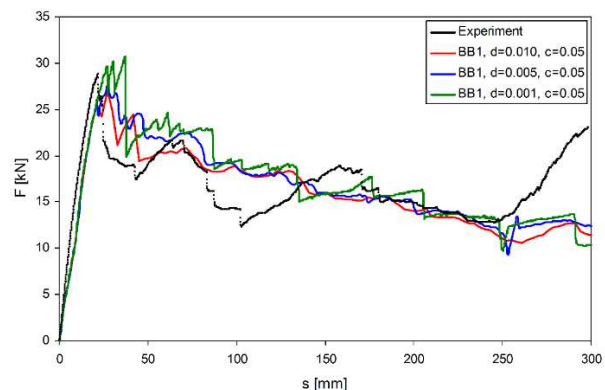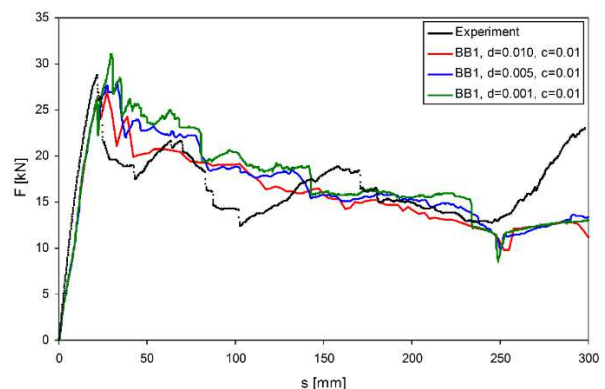Rys. 4. Wykresy $F(s)$ odpowiadające przyrostom d = 0.010, 0.005, 0.001 i tolerancji c = 0.10

Fig. 5. $F(s)$ graphs corresponding to increments d = 0.010, 0.005, 0.001 and tolerance c = 0.05

Rys. 5. Wykresy $F(s)$ odpowiadające przyrostom d = 0.010, 0.005, 0.001 i tolerancji c = 0.05
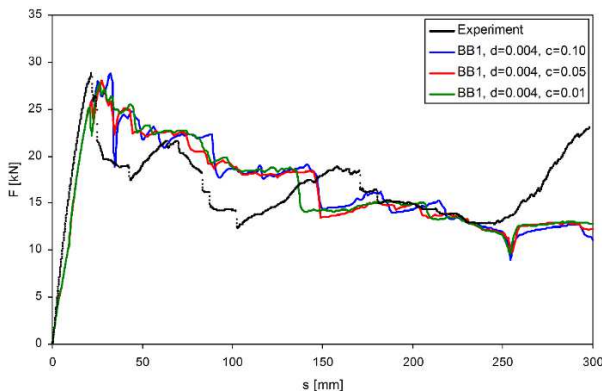

Fig. 6. $F(s)$ graphs corresponding to increments d = 0.010, 0.005, 0.001 and tolerance c = 0.01

Rys. 6. Wykresy $F(s)$ odpowiadające przyrostom d = 0.010, 0.005, 0.001 i tolerancji c = 0.01

Figure 7 shows $F(s)$ graphs corresponding to increment $d = 0.004$ and tolerances $c = 0.10, 0.05, 0.01$. Table 2 summarizes the F_{max} values (pressure force F at the load capacity point) and the corresponding values of displacement s of the crosshead. Differences in percent in relation to the experimental value are given in brackets. The results allow the $F(s)$ graph corresponding to the pair $d = 0.004$, $c = 0.05$ to be considered the best suited to the experimental graph in the quasi-linearly elastic response zone. This pair was adopted in further simulations.

Figure 8 shows $F(s)$ graphs for the three FE meshes. In the case of the rare mesh, correct estimation of the load capacity of the beam was not obtained, and with crosshead displacement $s = 262.8$ mm, no convergence was obtained. Table 3 presents the F_{max} values and the corresponding displacement s values for the analysed FE meshes. Differences in percent in relation to the experimental value are given in brackets. The results allow the $F(s)$ graph corresponding to the base mesh to be considered the most consistent with the experimental result.
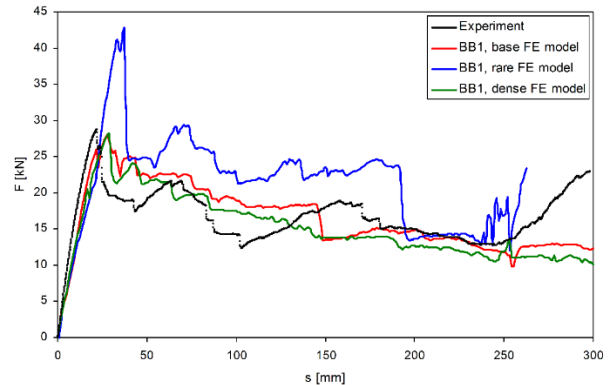

Fig. 7. $F(s)$ graphs corresponding to increments $d = 0.004$ and tolerances $c = 0.10, 0.05, 0.01$

Rys. 7. Wykresy $F(s)$ odpowiadające przyrostom $d = 0.004$ i tolerancji $c = 0.10, 0.05, 0.01$

Fig. 8. $F(s)$ graphs for different FE mesh densities

Rys. 8. Wykresy $F(s)$ dla różnych gęstości siatki ES

TABLE 2. **Values of force F_{max} at load bearing capacity point and corresponding values of displacement s of crosshead**

TABELA 2. **Wartości siły F_{max} w punkcie nośności oraz odpowiadające wartości przemieszczenia s trawersy**

d, c	F_{max} [kN]	s [mm]
0.010, 0.10	27.0 (–6.3%)	27.00 (22.6%)
0.010, 0.05	27.0 (–6.3%)	27.00 (22.6%)
0.010, 0.01	26.9 (–6.6%)	27.00 (22.6%)
0.005, 0.10	27.4 (–4.9%)	24.00 (9.0%)
0.005, 0.05	27.5 (–4.5%)	27.00 (22.6%)
0.005, 0.01	27.9 (–3.1%)	33.00 (49.9%)
0.004, 0.10	28.9 (0.3%)	32.40 (47.1%)
0.004, 0.05	28.1 (–2.4%)	27.60 (25.3%)
0.004, 0.01	27.7 (–3.8%)	26.40 (19.9%)
0.001, 0.10	34.1 (18.4%)	33.30 (51.2%)
0.001, 0.05	30.7 (6.6%)	37.20 (68.9%)
0.001, 0.01	31.1 (8.0%)	30.00 (36.2%)

TABLE 3. **Influence of FE mesh density on load bearing capacity point**

TABELA 3. **Wpływ gęstości siatki ES na punkt nośności**

Quantity	Exp.	Base mesh	Rare mesh	Dense mesh
F_{max} [kN]	28.8	28.1 (–2.4%)	42.7 (48.3%)	28.2 (–2.1%)
s [mm]	22.02	27.60 (25.3%)	37.20 (68.9%)	28.80 (30.8%)

SIMULATION RESULTS FOR BB1 MODEL

This section presents the full simulation results corresponding to the BB1 model (preferred), base mesh and simulation parameters $d = 0.004$, $c = 0.05$ determined in the previous section. The $F(s)$, simulation (with the above mentioned conditions) and experimental graphs were analysed in the previous section.

Figures 9 and 10 show the experimental and simulation deformation of the box beam at every 50 mm of vertical displacement of the crosshead of the universal testing machine. Very good qualitative and quantitative correlation of the deformation is visible and the conclusion about the underestimated shear modules G_{13}, G_{23} in the simulation is confirmed.

The power of CAE systems is based, among others, on the ability to determine total effort contour maps (TECM) maps, separately for laminate shells and adhesive layers. In the design, these maps allow one to specify the overload zones and add additional laminae in these zones. Figure 11 shows the TECM map for the laminate shells at the load capacity point. The imprint

For the BB1 model and the basic ply sequence, the effect of the finite element (FE) mesh density on the $F(s)$ graph was analysed. The FE mesh of the basic model was thinned twice and compacted twice. For a twice thinner FE mesh (rare mesh), the model has 2728 FEs (2772 nodes). For a twice denser FE mesh (dense mesh) there are 44352 FEs (44528 nodes) in the model.

of the crosshead pressure stamp of the testing machine as well as the transfer of the load to the supports are visible. The overload zones on the supports are many times smaller due to the two-fold smaller pressures and the two-fold thicker laminate on the beam flanges.
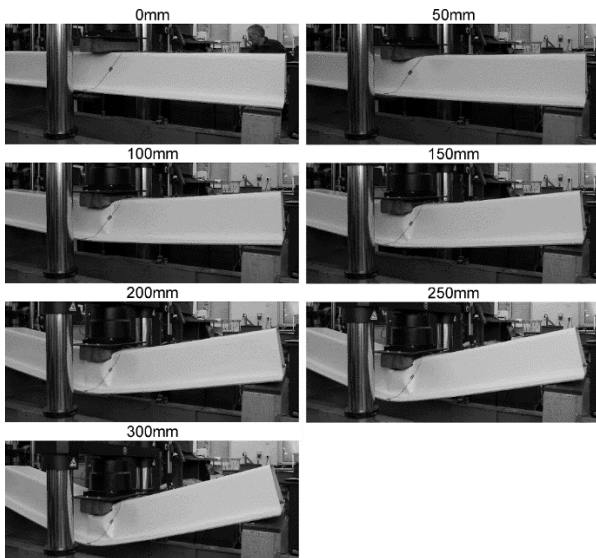

Fig. 9. Box beam deformation in experimental test

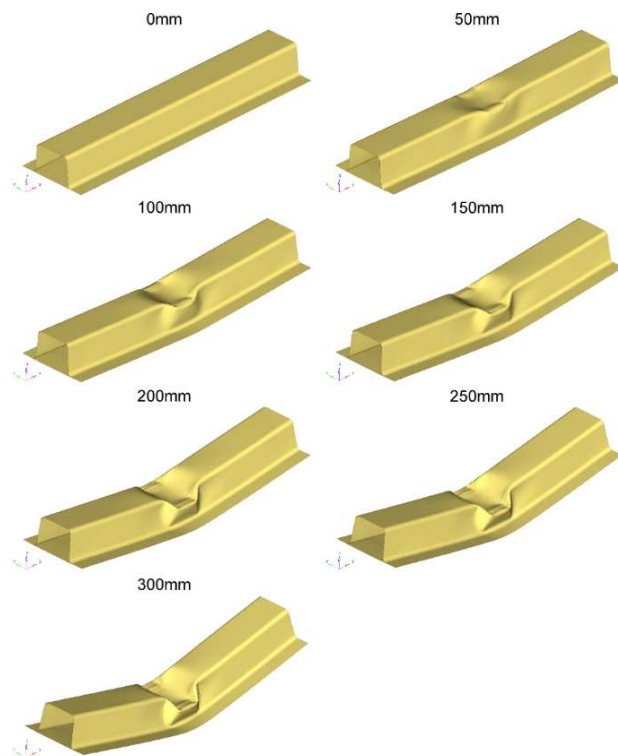Rys. 9. Deformacja belki skrzynkowej w teście eksperymentalnym

Fig. 10. Box beam deformation in simulated test (BB1 model)

Rys. 10. Deformacja belki skrzynkowej w teście symulacyjnym (model BB1)

Figure 12 shows the TECM map of the adhesive layers. The stresses in these layers are small. The geometry of the beam cross-section indicates that longitudinal normal stresses prevail in the adhesive layers and the remaining stress components are negligible.
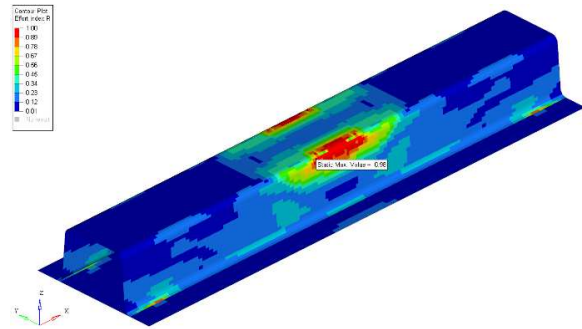

Fig. 11. ECM map for laminate shells with base sequence S1 (isometric view from top, scale 0-1)

Rys. 11. Mapa TECM dla powłok laminatowych z sekwencją podstawową S1 (widok izometryczny z góry, skala 0-1)
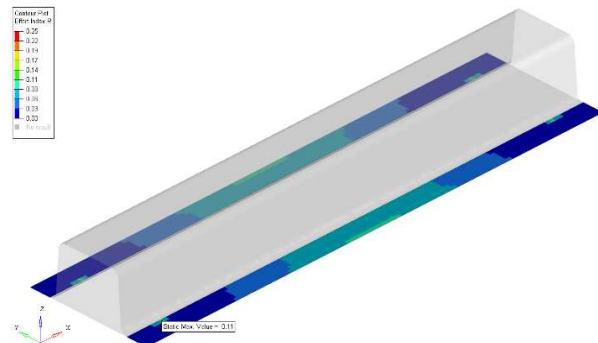

Fig. 12. TECM map for adhesive layers (sequence S1, isometric view from top, scale 0-0.25)

Rys. 12. Mapa TECM dla warstw klejowych (sekwencja S1, widok izometryczny z góry, skala 0-0.25)

After experimental validation of the numerical modelling and simulation methodology, quasi-optimization of the ply sequence was performed with the objective function as the maximum load bearing capacity of the beam. Quasi-optimization is limited to laminae used in the reference ply sequence and possible symmetric variants.

Five ply sequence variants of the laminate shells will be considered:

code S1: $[0/45/0_2/45/0]$ (reference ply sequence, experimental test)

code S2: $[0_2/45_2/0_2]$

code S3: $[45/0_4/45]$

code S4: $[45_6]$

code S5: $[0_6]$

Simulations of a three-point bending test of an adhesively bonded box beam were performed for the S2 ply sequence (GBX together in the middle of the laminates), S3 (GBX separately outside the laminates), S4 (GBX only), S5 (BAT only) and compared with base sequence S1 (GBX separately, symmetrically inside the laminates).

Figure 13 shows $F(s)$ graphs corresponding to the S1-S5 ply sequences. Table 4 summarizes the F_{max} force and the corresponding displacement s values for the tested ply sequences. Figures 14-17 show the TECM maps for the laminate shells at the load capacity point, corresponding to the remaining ply sequences,

being modifications to base sequence S1, i.e. S2, S3, S4, S5. The simulations correspond to the BB1 model, base mesh and simulation parameters $d = 0.004$, $c = 0.05$.
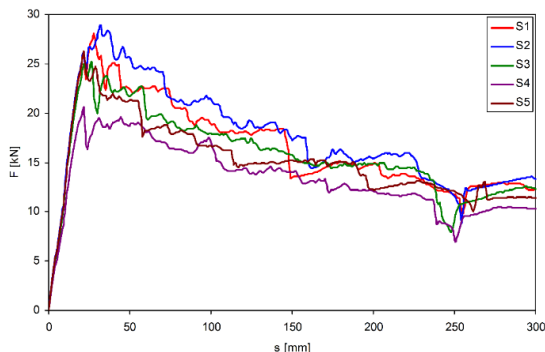

Fig. 13. $F(s)$ graphs for tested laminate shell ply sequences

Rys 13. Wykresy $F(s)$ odpowiadające testowanym sekwencjom warstw powłok laminatowych

TABLE 4. F_{max} force and corresponding displacement s values for tested ply sequences

TABELA 4. Wartości siły F_{max} i odpowiadającego przemiesz-czenia s dla testowanych sekwencji warstw

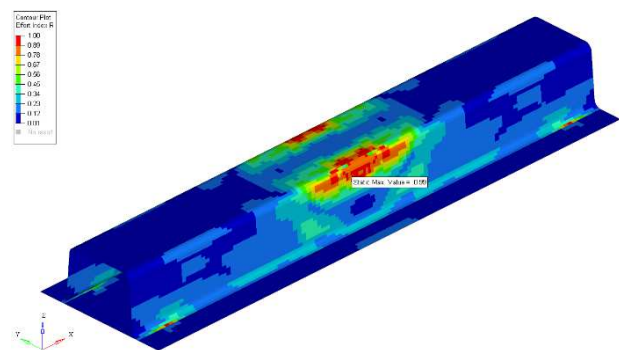| Quantity	Exp.	S1	S2	S3	S4	S5
F [kN]	28.8	28.1 (-2.4%)	28.9	25.1	20.5	26.3
s [mm]	22.0	27.6 (25.3%)	32.4	26.4	21.6	21.6

Fig. 14. TECM map in laminate shells with S2 sequence (isometric view from top, scale 0-1)

Fig. 14. Mapa TECM w powłokach laminatowych z sekwencją S2 (wi-dok izometryczny z góry, skala 0-1)
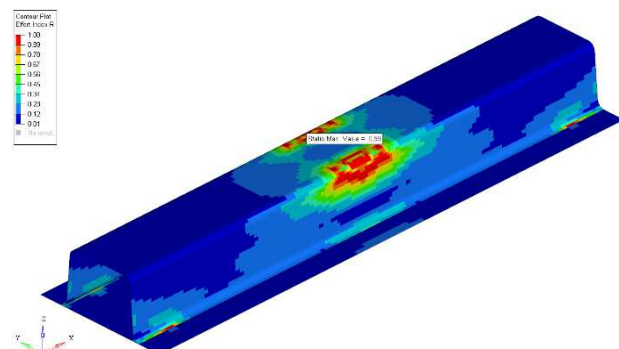

Fig. 15. TECM map in laminate shells with S3 sequence (isometric view from top, scale 0-1)

Rys. 15. Mapa TECM w powłokach laminatowych z sekwencją S3 (widok izometryczny z góry, skala 0-1)
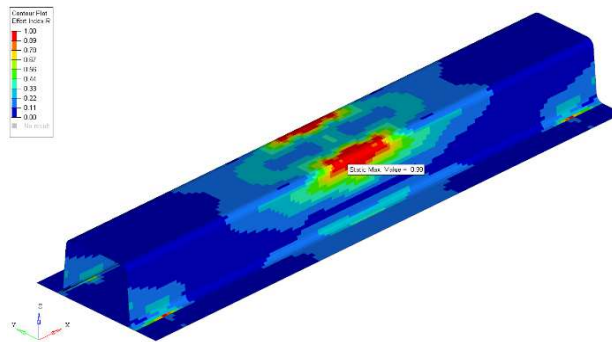
Fig. 16. TECM map in laminate shells with S4 sequence (isometric view from top, scale 0-1)

Rys. 16. Mapa TECM w powłokach laminatowych z sekwencją S4 (widok izometryczny z góry, skala 0-1)
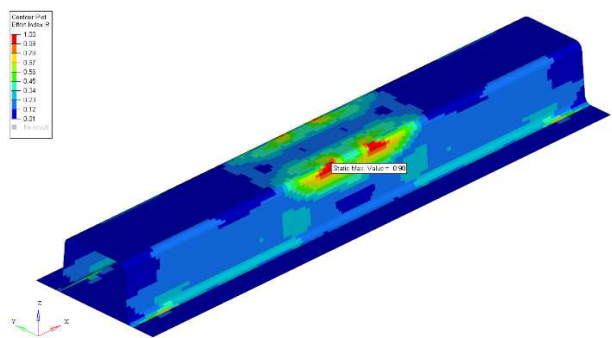

Fig. 17. TECM map in laminate shells with S5 sequence (isometric view from top, scale 0-1)

Fig. 17. Mapa TECM w powłokach laminatowych z sekwencją S5 (widok izometryczny z góry, skala 0-1)

Based on Figures 13-17 and Table 4, the following conclusions were made:
1. The flexural stiffness of beams with sequences S1, S2, S3, S4, S5 in the quasi-linearly elastic response zone up to 30% of the load capacity are similar.
2. The beam with the S2 sequence has the highest load capacity. It is a symmetrical sequence in which the number of BAT800 [0/90] fabrics is twice as large as the number of GBX800 [45/−45] fabrics. The GBX fabrics form the core of the laminate, and BAT fabrics - the laminate covers. Sequence S2 should be preferred in forming box beams in civil engineering.
3. The load capacity of the box beam for the S1 sequence is 2.8% smaller than the load capacity cor-responding to the S2 sequence. A further decrease in the load capacity is observed successively for the S5 sequence (by 9%), S3 (by 13.1%), S4 (by 29.1%). Composite beams in which only GBX800 [45/−45] is used should not be applied in civil engineering. These fabrics do not prevent creep in bent beams.
4. The progressive failure of beams with sequences S1, S2, S3, S4, S5 is similar.
5. The smallest damage of the top laminate shell under the pressing block corresponds to   sequence S5 (only BAT800 [0/90] fabrics). When forming com-posite box beams, the aim is to use the S2 sequence in the webs and the S5 sequence in the upper and lower belts of the I-beam.

SIMULATION RESULTS FOR BB2 MODEL

Figure 18 shows the *F(s)* simulation graph corresponding to the BB2 numerical model against the background of the experimental graph.
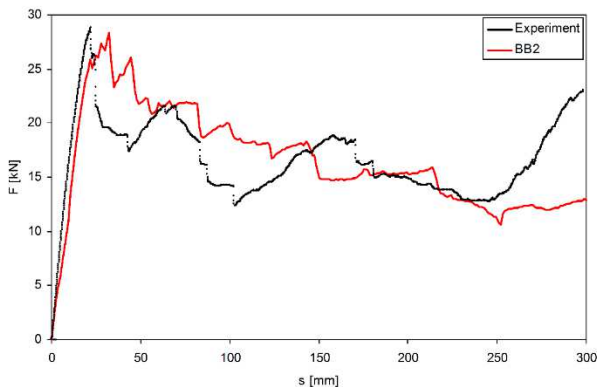

Fig. 18. *F(s)* simulation graph corresponding to BB2 model against background of experimental graph

Rys. 18. Wykres symulacyjny *F(s)* odpowiadający modelowi BB2 na tle wykresu eksperymentalnego

Comparison of the *F(s)* simulation graphs for the BB1 and BB2 models shows that both models give similar results, however, the results for the BB1 model can be considered better due to the smaller displacement errors in the load capacity point. Moreover, the BB2 model in which the *Glue* contact option was applied, does not take into account the thickness of the glued joints, nor does it give the possibility to determine the degree of effort of these joints. For these reasons, in engineering applications, the authors recommend the BB1 model in which the glued joints are modelled as an additional core layer of the laminate being a joint of two laminates.

CONCLUSIONS

The work is an experimental and numerical study of an adhesively bonded GFRP composite box beam, which reflects a central part of a footbridge superstructure designed by the authors. The beam was subjected to a three-point bending test. Due to contact with friction between the crosshead and the top laminate shell, contact with friction between the bottom laminate shell and the supports, as well as conducting testing also in the zone of progressive failure of laminates, the numerical task is non-linear physically and geometrically.

The MSC.Marc system and CAE supplementary software were used for numerical modelling and simulation of the three-point bending test of an adhesively bonded GFRP composite box beam. As a result of experimental validation of the numerical modelling and simulation of the beam, the parameters and options of modelling and simulation were determined, leading to the best simulation compatibility with the experiment in the quasi-linearly elastic zone and to fairly good agree-

ment in the progressive failure zone. The topology and formulation of finite elements, FE mesh density, convergence tolerance, iterative step, friction contact options, laminate and adhesive material models, as well as the laminate and adhesive failure models were determined.

It has been shown that better results are obtained by the BB1 model, which takes into account the thickness and deformation of the glued joints.

After the experimental validation of the numerical modelling and simulation, quasi-optimization of the ply sequence was conducted based on simulations of the three-point beam bending test, with the objective function as the maximum load bearing capacity of the beam. It has been pointed out that in forming box composite beams, it is beneficial to use the S2 sequence in the webs and the S5 sequence in the upper and lower belt of I-beam sections. In the S2 sequence stitched fabrics with the orientation [45/−45] with respect to the beam axis constitute the core of the laminate, and stitched fabrics with the orientation [0/90] are the laminate covers. In the S5 sequence, only stitched fabrics with the orientation [0/90] in relation to the beam axis appear.

Laminate shells reinforced with stitched E-glass fabrics were considered, made using modern ecological infusion technology. The parameters and options of numerical modelling and simulation of adhesively bonded GFRP composite shells determined in this work are recommended for detailed calculations in the design of civil engineering structures, including footbridges.

Acknowledgements

REFERENCES

[1] MSC.Marc 2010, Vol. A: Theory and User Information, Vol. B: Element Library, MSC.Software Co., Santa Ana, CA, USA, 2010.

[2] Kubiak T., Kaczmarek L., Estimation of load-carrying capacity for thin-walled composite beams, Composite Structures 2015, 119, 749-756.

[3] Kubiak T., Samborski S., Teter A., Experimental investigation of failure process in compressed channel-section GFRP laminate columns assisted with the acoustic emission method, Composite Structures 2015, 133, 921-929.

[4] Gliszczyński A., Kubiak T., Progressive failure analysis of thin-walled composite columns subjected to uniaxial compression, Composite Structures 2017, 169, 52-61.

[5] Klasztorny M., Bondyra A., Szurgott P., Nycz D., Numerical modelling of GFRP laminates with MSC.Marc system and experimental validation, Computational Materials Science 2012, 64, 151-156.

[6] Klasztorny M., Nycz D., Labuda R., Modelling, simulation and experimental validation of bend tests on GFRP laminate beam and plate specimens, Composite Structures 2018, 184, 604-612.

[7] Chroscielewski J., Klasztorny M., Miskiewicz M., Romanowski R., Wilde K., Innovative design of GFRP sandwich footbridge. In: Footbridge 2014, 5th International Conference on Footbridges: Past, Present & Future, London, England, 16-18 July 2014, Ed. L. Debell, H. Russel, USB Proceed., Paper #1250, 1-8.

[8] Klasztorny M., Chróścielewski J., Szurgott P., Romanowski R., Design and numerical testing of 5-box GFRP shell footbridge. In: Footbridge 2014, 5th International Conference on Footbridges: Past, Present & Future, London, England, 16-18 July 2014, Ed.: L. Debell, H. Russel, USB Proceed., Paper #1094, 1-8.

[9] Klasztorny M., Nycz D., Cedrowski M., Modelling, simulation and validation of bending test of box segment formed as two composite shells glued together, Composites Theory and Practice 2015, 15(2), 88-94.

[10] Banea M.D., da Silva L.F.M., Adhesively bonded joints in composite materials: an overview, Proc. IMechE Vol. 223, Part L: J. Materials: Design and Applications, JMDA219 © IMechE 2009, 1-18, DOI: 10.1243/14644207JMDA219.

[11] Vallée T., Tannert T., Meena R., Hehl S., Dimensioning method for bolted, adhesively bonded, and hybrid joints involving fibre-reinforced-polymers, Composites Part B: Engineering 2013, 46, 179-187.

[12] Klasztorny M., Nycz D.B., Romanowski R.K., Gotowicki P., Kiczko A., Rudnik D., Effects of operating temperature and accelerated environmental ageing on glass-vinylester composite mechanical properties, Mechanics of Composite Materials 2017, 53(3), 335-350.